Bio-Hybrid Tumor Cell-Templated Capsules: A Generic Formulation Strategy for Tumor Associated Antigens in View of Immune Therapy

*Lien Lybaert, Elly De Vlieghere, Riet De Rycke, Nane Vanparijs, Olivier De Wever, Stefaan De Koker, and Bruno G. De Geest**

For the development of effective anti-cancer vaccines, tumor associated antigens need to be internalized by antigen presenting cells alongside specific co-stimulatory signals. Interestingly, relative to soluble antigens, nano- and micro-particulate antigens are much better presented to CD8 T cells, a crucial step in the induction of cytotoxic T cells that can eliminate malignant cells. In this regard, a generic strategy to encapsulate cancer cell derived proteins into a particulate delivery system would be of high interest. Here we present a versatile approach to incorporate cancer cell proteins into polymeric capsules using the cells themselves as templates for layer-by-layer assembly of complimentary interacting species. After coating, the cells are killed by hypo-osmotic treatment leading to bio-hybrid capsules loaded with cell lysate. Particular focus is devoted in this work on choosing the optimal coating components and conditions to maximize cell membrane integrity during the coating process, minimize pre-mature protein release and achieve optimal encapsulation of cell lysate upon lysis of the cells. To further underline the generic nature of our approach, we demonstrate that heat shock proteins, important immune-activators, can be induced and encapsulated into the bio-hybrid capsules.

1. Introduction

Despite major research effort in cancer research, there remains a great need for more specific and targeted therapies to combat metastatic disease and to reduce the need for traditional chemo- and radiotherapies that are both prone to serious side effects.[1–3] Anti-cancer immune-therapy involves priming the patient's own immune system to recognize and eliminate malignant cells. It is currently recognized as one of the most promising strategies for the treatment of metastatic cancer.[4] To achieve targeted treatment, tumor associated antigens have to be internalized by dendritic cells (DCs; the most potent class of antigen presenting cells of the immune system) and presented to CD8 T cells in combination with the appropriate cytokine spectrum and co-stimulatory signals.[1,2,5,6] Subsequent differentiation of CD8 T cells into cytotoxic T cells (CTLs) provides the required killer T cell force for tumor eradication.[7]

However, CD8 T cell presentation is normally restricted to endogenous antigens, i.e., antigens expressed within the cytoplasm of DCs themselves, and is highly inefficient for exogenous antigens that typically become presented by DCs via a MHC-II peptide complex to CD4 T cells.[5,8] Therefore, strategies that promote presentation of exogenous tumor associated antigens to CD8 T cells via MHC-I, a process termed cross-presentation, are highly desired in view of anti-cancer immune therapy.[8–10] Recent advances at the interface between immunology and materials chemistry have elucidated that formulating protein-based antigens into particulate carriers in the range of 50 nm – 10 µm strongly promote cross-presentation by DCs to CD8 T cells.[9–15] These findings provide a clear rationale to design strategies for the delivery of tumor associated antigens in particulate form to DCs.

Unfortunately, encapsulation strategies for tumor-associated antigens are limited as antigens of many cancer types are still unidentified on the one hand and are also prone to continuous mutation on the other.[16,17] To overcome these limitations, we detail an approach to encapsulate tumor associated antigens by templating a synthetic membrane onto the surface of cancer cells followed by lysis of the cancer cells retaining cell lysate within the hollow void of the obtained capsules (**Figure 1**A). Cell encapsulation has not yet been used for

L. Lybaert, N. Vanparys, Dr. S. De Koker, Prof. B. G. De Geest
Department of Pharmaceutics
Ghent University
Ottergemsesteenweg 460, 9000 Ghent, Belgium
E-mail: br.degeest@ugent.be
E. De Vlieghere, Prof. O. De Wever
Laboratory of Experimental Cancer Research
Ghent University, De Pintelaan 185
9000 Ghent, Belgium
R. De Rycke
Department of Biomedical Molecular Biology
IRC, Ghent University
Technologiepark 927
9052 Zwijnaarde, Belgium
R. De Rycke, Dr. S. De Koker
Department of Molecular Biomedical Research
VIB, Ghent University Technologiepark 927
9052 Zwijnaarde, Belgium

DOI: 10.1002/adfm.201402303

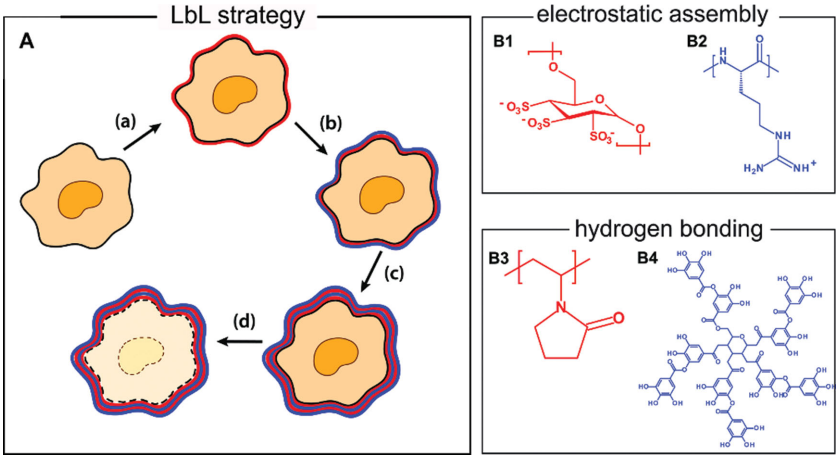

Figure 1. Schematic representation (A) of the design of LbL-coated bio-hybrid cancer cell-templated capsules with alternating layers (step a-c) of either the electrostatically interacting polyelectrolytes dextran sulfate (B1) and poly-L-arginine (B2) or poly(N-vinylpyrrolidone) (B3) and (B4) tannic acid that interact via hydrogen bonding followed by lysis of the cells upon hypo-osmotic treatment (step d).

anti-cancer immunotherapy but has found applications in several biomedical applications including tissue engineering and diabetes treatment.[18–21] Current progress on implementing whole cell lysates as anti-cancer vaccine is mostly based on ex vivo DC therapy, involving electroporation of DCs derived from the cancer patient's own blood monocytes.[22,23] This is a highly costly labor-intensive procedure and does not take advantage of the physiological stimuli that occur in direct in vivo vaccination and therefore urges for viable alternatives.[4,24]

By employing in vivo targeting of autologous tumour cell lysate, the patient's individual tumour-specific and/or tumour associated antigens can be delivered to the immune system in an immunogenic fashion, which should enable the induction of broader immune responses specifically tailored to the patient's unique tumour mutanome.[16,17] However, one might argue that immunisation of cancer patients with a vaccine containing autologous tumour cell lysate could lead to induction of autoimmunity against cellular proteins that are shared with normal cells. However, this has, at least to our knowledge, not yet been reported in both preclinical and clinical studies.[25–28]

Layer-by-Layer (LbL) assembly of complementary interacting components is an attractive technique to deposit a semi-permeable membrane on the surface of non-planar substrates.[29] It allows an easy, all-aqueous mild encapsulation of a wide variety of species, mostly polymeric or inorganic template particles that are used to design hollow capsules. Several studies have already been reported on LbL coating of cells mainly focussing on encapsulation of living yeast cells or bacteria.[20,30–32] However these microbial cells are more robust due to their rigid cellular wall whereas mammalian cells are more fragile.[33] Here we present the LbL encapsulation of murine melanoma B16.F10 cells, as model cancer cell line, aiming at high preservation of the cell membrane integrity and good protein retention contained within the deposited multilayer coating.

2. Results and Discussion

2.1. Screening the Interaction Between Cells and Oppositely Interacting Species

Due to the overall negative charge of the cell membrane, we attempted at first to coat B16.F10 melanoma cells based on electrostatic interaction of the oppositely charged polyelectrolytes poly-L-arginine (P_LARG) (Figure 1B1; polycation) and dextran sulfate (DEXS) (Figure 1B2; polyanion). This choice is based on our previous work where we showed multilayer capsules composed of these polyelectrolytes are biocompatible, degradable in vitro[34] and in vivo[35] and induce broad cellular and humoral immune responses against encapsulated antigen.[36–38] However, whereas in the form of a polyelectrolyte complex poly-L-arginine is not inducing acute cytotoxicity,[39] we observed that incubation of live cells in a poly-L-arginine solution at a relevant concentration for Layer-by-Layer assembly (i.e., 0.1 to 1 mg/mL in isotonic HEPES buffer) induces instantaneous aggregation, cell lysis and cell death (vide infra and **Figure 2**). Therefore, we were prompted at investigating an alternative for electrostatic assembly to assure a better preservation of cell viability during cell coating. In this regard, hydrogen bonding is attractive because it involves non-ionic species and particularly hydrogen bonded thin films composed of tannic acid (TA; Figure 1B3) and neutral charged hydrophilic polymers such as e.g., poly(vinylpyrrolidone) (PVP, Figure 1B4) have recently attracted interest.[31,32,40] Although PVP and TA form strong complexes, PVP/TA multilayers have been reported to gradually disassemble over time, likely due to oxidation, and is therefore an attractive system for delivery purposes.[41,42] Additionally we have recently reported the design of porous microparticles based on TA/PVP via spray drying.[43] These particles were used to encapsulate protein antigens and we successfully demonstrated that the antigens, after cellular uptake, could still be processed together with a dramatic increase in cross-presentation. This suggests that in intracellular conditions, proteases are still granted access to the payload that is firmly entrapped within the particles under extracellular conditions. Tannic acid is a safe food-grade compound that is applied in biomedical applications including haemostatic coatings, nanocapsules and cell encapsulation. Besides via hydrogen-bonding, tannic acid has also shown its capability to form thin films via multiple mechanisms.[44,45] PVP is a non-ionic polymer that is approved by the FDA for pharmaceutical applications.

As the aim of our work is to encapsulate whole cancer cells it is important to preserve cell integrity as much as possible while affecting cell viability as little as possible in order to retain a maximum amount of cellular proteins within the LbL coating. Therefore, in a first series of experiments, we investigated the effect of incubating cells in isotonic aqueous solution of respectively DEXS, P_LARG, TA and PVP on cell integrity and

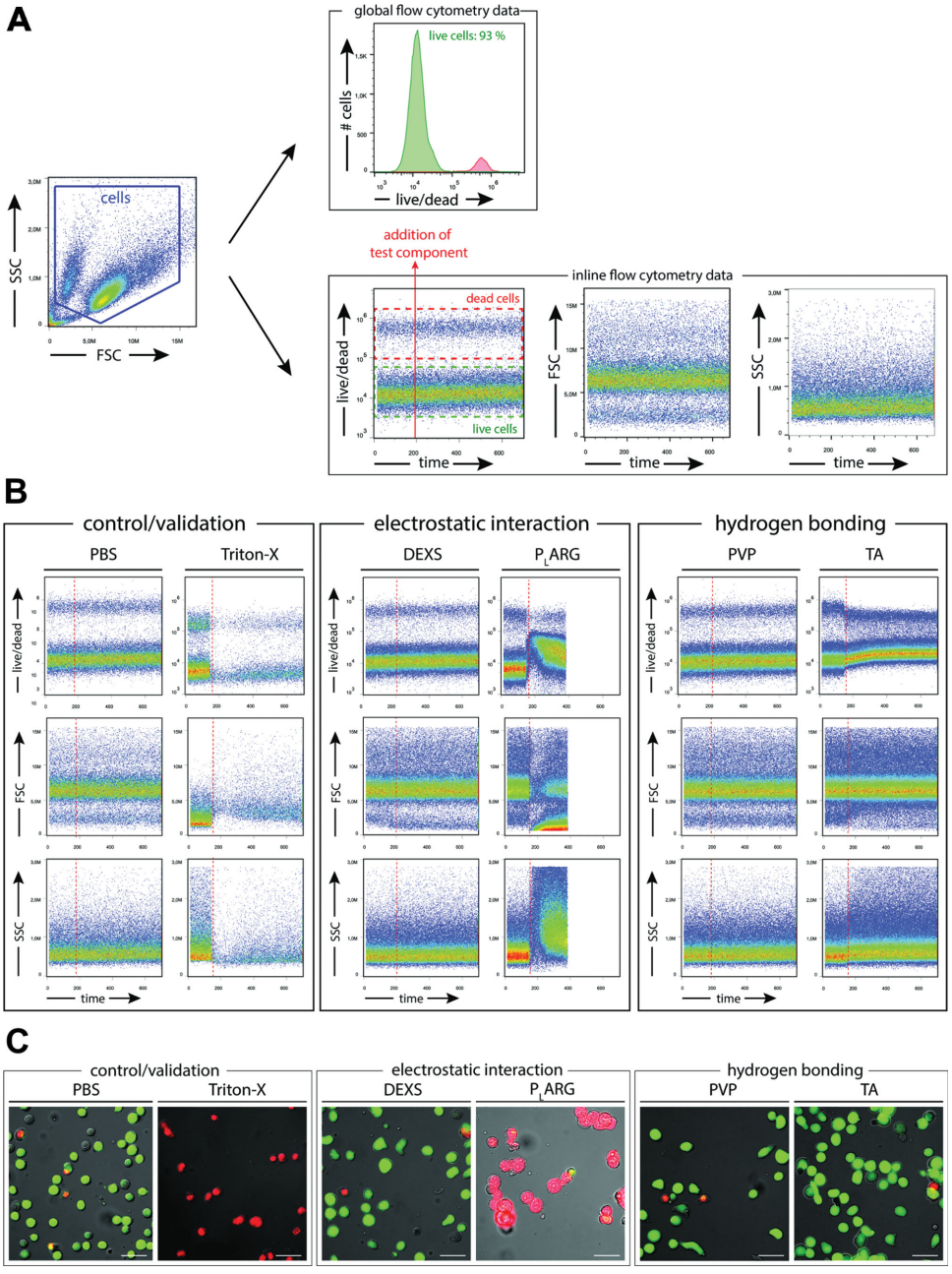

Figure 2. A) Flow cytometry gating strategy for determination of B16.F10 cell viability offline and inline. B) Inline flow cytometry data representing the response to the addition of the respective test components in the FL-3 fluorescence channel (live/dead staining and the forward (FSC), respectively side (SSC) scatter channels. The dashed red line indicates the time points at which the test components were added. C) Fluorescence microscopy images of B16.F10 cells staining with C-AM/PI after 10 min. incubation with the respective test components on ice. Overlay of the DIC, green and red fluorescence channels. Scale bar is 50 µm.

cell viability. For this purpose B16.F10 cells were incubated in 1 mg/mL HEPES-buffered solutions of either P_LARG or DEXS while on the other hand the B16.F10 cells were incubated in PBS buffered 1 mg/mL solutions of either TA or PVP. HEPES buffer is used to solubilise DEXS and P_LARG as the latter is not soluble in PBS due to ionic crosslinking of the cationic guanidinium moieties of the P_LARG by the trivalent phosphate anions of the PBS buffer. To avoid active phagocytosis of these components during the coating process, all handlings were performed on ice to block energy-dependent internalization pathways.

The effect of the respective test components on cell viability and membrane integrity was subsequently assessed by inline flow cytometry (FACS) in presence of a live/dead stain (Figure 2). This technique comprises continuous sampling/measuring of a cell suspension while adding the test component of choice at a certain point to probe for the effect on cell viability. In addition, the flow cytometry observations were

supported by visualization of the cytotoxicity by staining the B16.F10 cells with calcein-AM (C-AM) and propidium iodide (PI). C-AM is a cell-permeable dye that is converted by esterases into a non-cell-permeable state upon cellular uptake. As such, it strongly stains live cells. PI intercalates with double-stranded DNA, as found in the cell nucleus, but is cell impermeable. PI will thus only stain the nuclei of cells that have a damaged cell membrane and is therefore used as a probe for cell membrane integrity.

The gating strategy applied to analyze the inline flow cytometry experiments is shown in Figure 2A. Here we deliberately did not gate out (by plotting FSC-A vs FSC-H and SSC-A vs SSC-H) doublets or multiplets (i.e., clusters of multiple cells instead of single cells) thus allowing us to probe possible induction of cell aggregation upon addition of the test component to the cells during the flow cytometry measurements. The first gate (forward scatter versus side scatter) serves to select both live and dead cells and to exclude cell debris. These two populations are marked by respectively a green (live cell) and a red (dead cells) dashed rectangle. In this regard, as shown in the second gate, it is important to realize that when performing in vitro cell culture experiments, always a small amount of dead cells is present. The next step in the gating strategy is plotting the fluorescence channel used for the detection of live/dead staining (i.e., FL-3) as function of time. To gather additional information on the cellular response to addition of the respective test components, we also plotted the forward (FSC) and the side (SSC) scatter channel as function of time. The panels B in Figure 2 represent the evolution over time of the live/dead signal of cells present in the gate that contains both live and dead cells. The measurement was started at time point zero and the test components were added after 2 minutes. To validate the set-up, we used PBS and Triton-X (i.e., a detergent that solubilizes the cell membrane) as controls. PBS is expected to not affect the cell viability, while Triton-X should immediately kill the cells. Indeed, the inline flow cytometry plots in Figure 2B, do not indicate any alternation in the signal as function of time when PBS is added. By contrast, Triton-X dramatically changes the response in FL-3, FSC and SSC channels combined with a strong decrease in numbers of events immediately after addition of Triton-X, indicating massive cell death and cell lysis.

Subsequently, we evaluated the influence on cell membrane integrity upon addition of the components that are of interest for Layer-by-Layer coating. DEXS did not influence the fluorescence signal. This is also confirmed by the corresponding fluorescence microscopy images in Figure 2C, recorded from an identically treated cell suspension as for the inline flow cytometry. Clearly, the majority of the cells exhibit strong green fluorescence by C-AM staining and only few are stained red by PI. By contrast, addition of P_LARG causes an immediate distortion of the fluorescence and scattering signals. Observation of clogging of the tubing due to aggregating cells (evidenced by the sharp decrease in FSC and increase in SSC signal), forced us to abort the measurements. The corresponding fluorescence microscopy images (Figure 2C) confirmed the aggregation and the nuclear staining with PI suggests that the majority of the cells have indeed lost their membrane integrity. When the inline flow cytometry experiments were performed with TA or PVP, no loss of cell viability/integrity was observed by either flow cytometry or microscopy. These data point out the superior performance of TA and PVP, compared to polyelectrolytes, to encapsulate cells in a polymeric multilayer coating while maintaining membrane integrity as much as possible and affecting cell viability as little as possible. Remarkably, in case of TA, a slight increase in the fluorescence signal from the live cell population whereas the dead cell population slightly decreases in signal upon addition of this component. Moreover, the FSC and SSC signals appear slightly altered. Although it is most likely that tannic acid interacts via hydrogen bonding with cell surface proteins or the live/dead stain, the exact reason for this subtle shift in fluorescence remains unclear.

Next, we also assessed the cellular viability/integrity with (common offline) flow cytometry (Figure 2A) comprising live/dead measurements after deposition of the test components and two washing steps to remove non-adsorbed material (Figure 2A). However, one might argue that in case cells completely lose their integrity or in case cells are lost during the multiple steps of pipetting, washing and centrifugation, they can no longer be stained by any of the dyes used in the previous experiments (i.e., live/dead, C-AM and PI). By consequence, these would neither be included in the amount of dead cells nor in the total cell number, and thus give rise to an overestimation of the cell viability. In order to address this issue we performed a MTT cell viability assay on B16.F10 cells that were incubated for 10 min on ice with the respective test components. MTT assay probes for the metabolic activity of cells by measuring the enzymatic conversion (which can only by performed by viable cells) of the substrate 3-(4,5-dimethylthiazol-2-yl)-2,5-diphenyltetrazolium bromide into the purple-colored formazan. As such, relative to a blank control, this assay quantifies the percentage of live cells taking into account the possible lost cells due to induced lysis by the test component or the multiple washing/centrifugation steps the cells are exposed to. **Figure 3** summarizes these measurements and compares the values obtained by live/dead staining and MTT assay. Clearly, the observed trends correspond well for both techniques, with only a slightly lower cell viability/integrity measured by MTT assay. Besides being independent of fully disintegrated cells and a small amount of cells that were aspirated when pipetting during washing and centrifugation, another difference between the MTT assay is that the latter requires, after pulsing and removal of the test component, an additional 2 h incubation

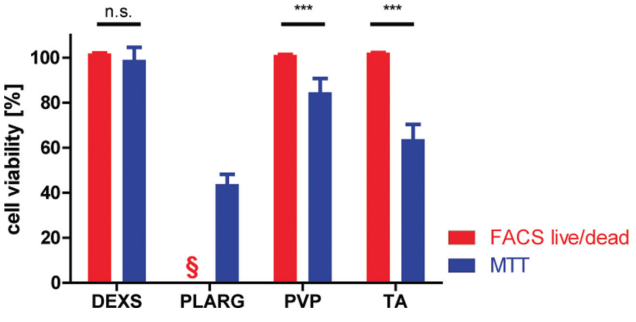

Figure 3. Cell viability/integrity, measured via MTT and FACS live/dead assay, measured after 10 min incubation of B16.F10 cells on ice with the respective test components. n = 6. ***: $p < 0.001$. §: FACS live/dead analysis was not possible due to massive cell aggregation.

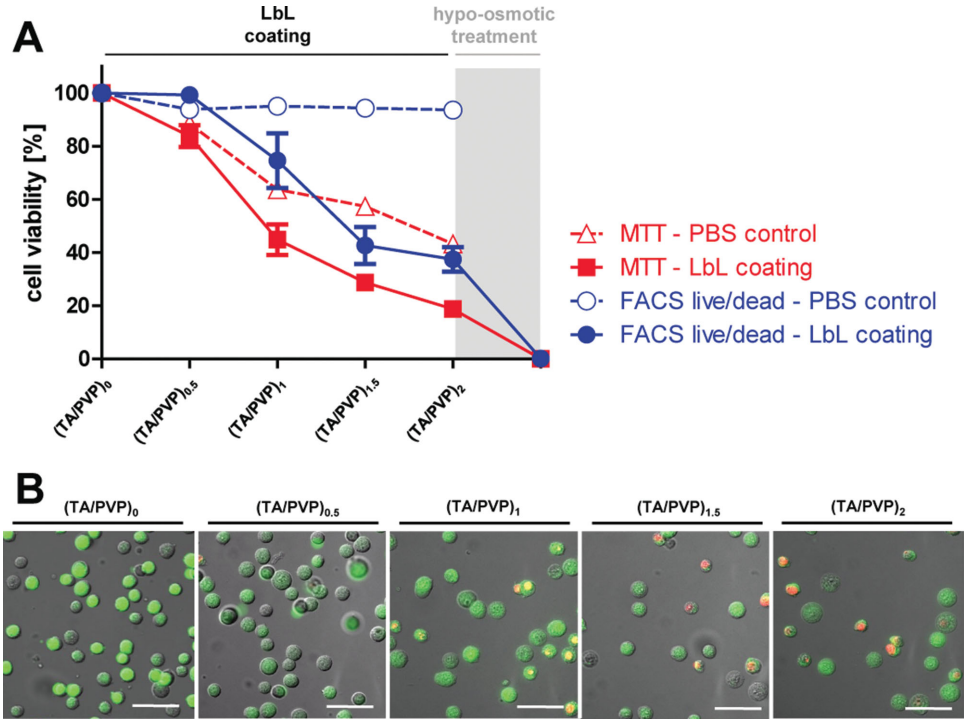

Figure 4. A) Cell viability, measured via MTT and FACS live/dead assay, measured after each deposition cycle during LbL coating of B16.F10 cells. The images are an overlay of the DIC, green and red fluorescence channels. N = 3. B) Fluorescence microscopy images of B16.F10 cells staining with C-AM/PI after each deposition cycle during LbL coating of B16.F10 cells. The images are an overlay of the DIC, green and red fluorescence channels. Scale bar is 50 μm.

period of the cells with the MTT substrate. As such, the cell viability/integrity measured by MTT assay probes for longer-term effect than the online FACS live/dead assay that depicts the immediate cellular response to the respective test compounds. Deeper investigation into this phenomenon is beyond the scope of this work. However, generally we can conclude that the inline flow cytometry set-up is a straightforward method to assess the instantaneous cellular response to a specific test component.

2.2. Characterization of the LbL Coating

Based on our initial flow cytometry and microscopy findings, we next attempted to coat the B16.F10 cells with a multilayer film by alternated assembly of TA and PVP. For this purpose, cells were sequentially incubated in 1 mg/mL solutions of respectively TA or PVP in PBS buffer. Also in these experiments, all handlings were performed on ice to block energy-dependent internalization pathways. After deposition of each layer, the cells were centrifuged and washed two times with PBS buffer to remove non-absorbed material. An important aim in this work is to measure the effect of these handlings on cell viability and more importantly on cellular integrity. Therefore, before dispersion of the cells in the respective coating solutions, cell viability/integrity was monitored by optical microscopy (C-AM/PI staining), FACS (live/dead staining) and MTT assay.

As repeated incubation on ice, pipetting, washing and centrifugation steps might have an effect, we also performed control experiments by subjecting cells to the same regime of handlings, but fully in PBS instead of using the respective coating components. The evolution of the cellular integrity/viability (monitored by either MTT or FACS live/dead) of these control groups is represented by the dashed curves in **Figure 4**A. FACS live/dead assay does not point out any significant cell death during repeated washing/centrifugation, whereas MTT assay does indicate a significant loss. Again, as discussed in the previous paragraph, this can likely be attributed to the longer time that is required to perform the MTT assay, to the small fraction of cells that is aspirated during the centrifugation/washing cycles and to possible induced cell lysis by the test component. In view of these findings future research will focus on novel strategies, thereby reducing loss of cell viability and membrane integrity, that allow one-step coating of cells based on novel concepts that were recently introduced into the field of colloidal engineering.[44,46]

The non-dashed curves in Figure 4A, represent the evolution of cell viability/integrity during LbL coating of the B16.F10 cells and indicate a gradual decrease as function of time. MTT and FACS live/dead assay show a similar trend that is confirmed by the microscopy images, as shown in Figure 4B, indicating increasing amounts of dead cells when depositing more layers. Importantly, no massive cell lysis or aggregation is observed during LbL coating of the cells. Figure 4A also represents the effect of a hypo-osmotic treatment on the cell viability/integrity. Previous studies on LbL coating of living cells describe cell survival of approximately 80% up to 95%.[32,47] Our results show however a dramatic reduction in cellular viability/integrity after

deposition of 2 bilayers. We assume this can be attributed to the different approach we elaborated on in our present work to assess the effect of LbL coating on cell integrity. So far in literature either yeast cells or bacteria, both having a rigid cell wall, have been used for LbL coating or cell viability/cell membrane integrity has been monitored solely after deposition of the entire LbL coating.[32,47,48] The latter thus excludes the extent of cell death or lysis that occurs during the coating process itself, which appears, at least in our hands, to play an important role.

2.3. Assessing the Influence of the Starting Layer on Cellular Integrity

Next we also aimed at investigating the effect of the starting layer (i.e., TA or PVP) on cellular integrity. Interestingly, when the Layer-by-Layer coating was initiated from PVP rather than TA, maintenance of the membrane integrity was improved as measured both by flow cytometry and MTT assay (**Figure 5**A). This suggests that using TA as starting material for cell-templated LbL assembly gives rise to an increased cytotoxicity upon further LbL coating. Although PVP is known for its non-fouling behavior, exhibiting only very low interaction with the cell surface, we observed that starting Layer-by-Layer assembly with PVP afforded a better preservation of the membrane integrity during the coating process. Further insight in how the cell surface is affected by incubation of the cells with a bilayer coating either initiated with PVP or TA, was gained by transmission electron microscopy (TEM). For this purpose cells were coated with a $(PVP/TA)_2$ or a $(TA/PVP)_2$ coating, fixated and embedded in epoxy resin. Figure 5B shows the TEM images recorded from ultrathin sections cut from the epoxy-embedded cells. These images clearly demonstrate the formation of an electron dense layer surrounding the cells and thereby confirm successful

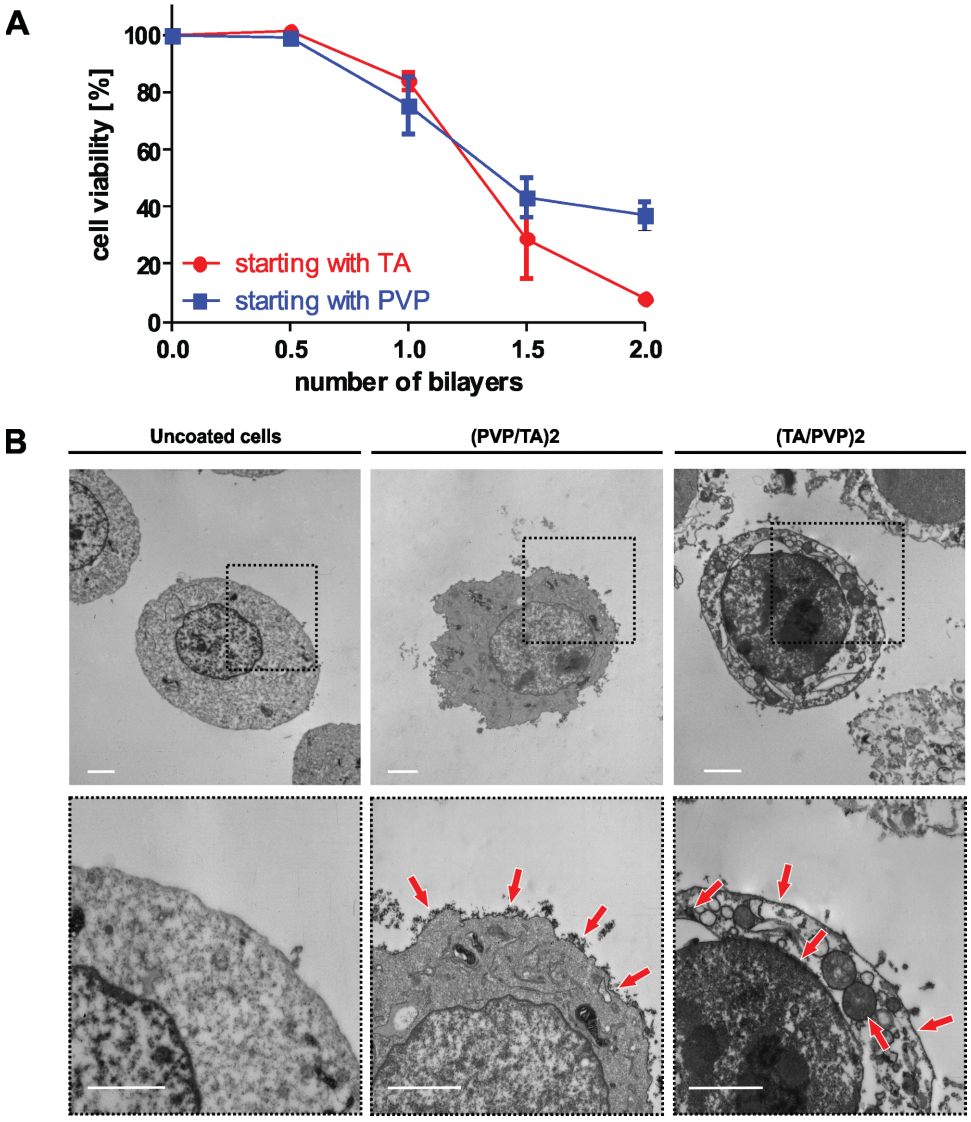

Figure 5. A) Cell viability, measured by a FACS live/dead assay, after each deposition cycle during LbL coating of B16.F10 cells. LbL coating was started with either TA (red curves) or PVP (blue curves). N = 3. B) TEM images of B16.F10 cells coated with 2 bilayers initiated with either TA or PVP compared with uncoated cells. The dashed rectangles show a zoomed area. Scale bar is 2 μm. The red arrows indicate the LbL coating.

deposition of the coating on the cell surface. Interestingly, when comparing cells coated with a $(PVP/TA)_2$ versus a $(PVP/TA)_2$ membrane, a dramatic difference in morphology of the resulting cell-templated capsules is observed. In case of $(PVP/TA)_2$ coated cells, the electron dense coating was confined to the surface of the cells, whereas in case of a $(TA/PVP)_2$ coating, electron dense material was found to be spread throughout the interior of the capsules as well (indicated by the red arrows). These findings support the live/dead flow cytometry data, suggesting that, TA partially crosses the cell membrane thereby creating pores in the cell membrane and thus enabling the uptake of the live/dead dye PI. Contrary, when cells are first incubated with PVP, only a coating on the cell surface is deposited, suggesting that adsorption of PVP onto the cell surface in a first step prevents cellular infiltration of TA in subsequent steps of the cell-coating process.

To gain further high resolution morphological insight into the cellular response to TA and PVP during Layer-by-Layer coating of the B16.F10 cells, TEM images (**Figure 6**) were recorded after deposition of each layer, either starting LbL assembly with PVP or TA. When LbL coating is started with TA, the morphology of the cells changes already after addition of the first TA layer, witnessed by the presence of an abnormal amount of vesicles (orange arrows). This indicates immediate cellular toxicity, likely attributed to tannic acid that crosses the cell membrane. In addition, the extent of swollen ER (blue) and mitochondria (yellow arrows) gradually increases as function of the number of deposited layers. Finally, after two TA/PVP

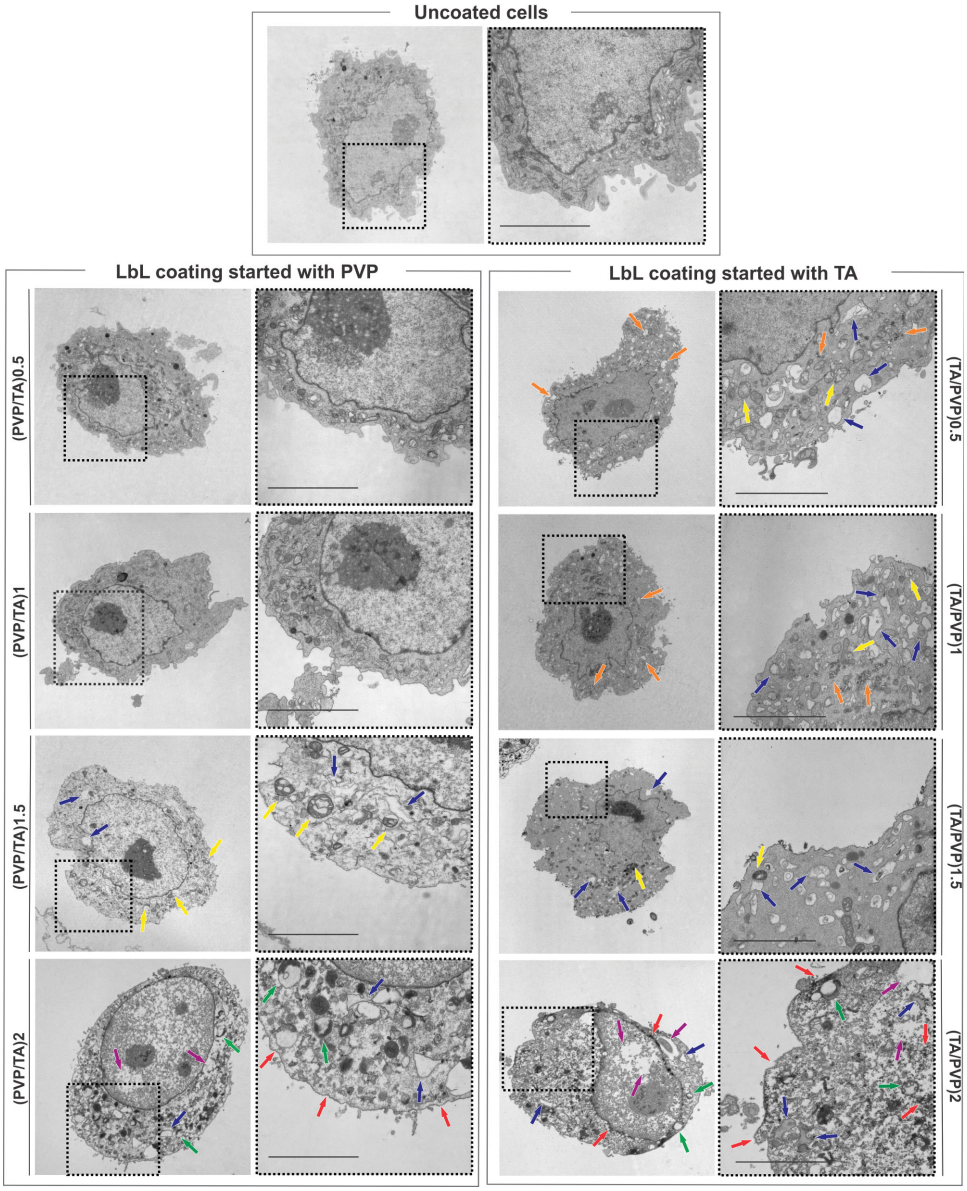

Figure 6. TEM images of B16.F10 cells coated with 1 to 4 alternating layers of PVP and TA, either started with PVP (left panels) or TA (right panels). The dashed rectangles show a zoomed area. Scale bar is 3 μm. The arrows indicate different cell structures: Orange = vesicles, Yellow = swollen mitochondria, Blue = swollen ER, Green = lysosomes, Purple = cell degeneration. The red arrows indicate the LbL coating.

bilayers, the cells exhibit a high amount of lysosomes (green arrows), i.e., degeneration remnants of the mitochondria, along with a high extent of degeneration of the cytoplasm and the cell nucleus (purple arrows). This can probably be attributed by the presence of additional pores in the plasma- and nuclear membranes together with the presence of the electron dense PVP/TA material (red arrows) on the cell surface and inside the cell.

Contrary, when the LbL coating is started with PVP, the cells exhibit a normal morphology after deposition of the first (i.e., $(PVP/TA)_1$) bilayer as the morphology of the cells appears to be unchanged compared to uncoated cells. However, during the position of the third layer (i.e., $(PVP/TA)_{1.5}$) the cell morphology starts to change, witnessed by the presence of swollen endoplasmatic reticulum (ER), swollen mitochondria and lysosomes, indicated by respectively blue, yellow and green arrows.

After deposition of two PVP/TA bilayers, the cellular degeneration process appears less pronounced than when LbL coating was started from TA and no PVP/TA complexes are observed inside the cells. However, also in this case an increased amount of abnormal cell structures together with initial degeneration of the cytoplasm and the cell nucleus (depicted by the purple arrows) are observed. These findings support our previous observations on membrane integrity (Figure 5A), where we observed a gradual increase of PI uptake in function of the alternating deposition cycles.

2.4. Determination of the Optimal Amount of Layers for Maximum Protein Retention

After establishing the feasibility of coating B16.F10 cells with a PVP/TA coating, starting with PVP as a first layer, we aimed at investigating the number of layers that is required to minimize protein release from the bio-hybrid capsules after lysis of the coated cells. For this purpose, after deposition of each layer, we exposed the cells to a hypo-osmotic medium by incubating them in deionized water. This treatment is intended to induce cell death in a facile and elegant way without addition of specific chemicals. As shown in Figure 4A, both MTT and FACS live/dead assay prove that the hypo-osmotic treatment effectively kills the cancer cells as no viable cells were detected anymore by both techniques. The effect of this treatment on cell integrity (i.e., by C-AM/PI staining) and on the morphology of the bio-hybrid capsules was subsequently evaluated by fluorescence microscopy (**Figure 7**A). In addition, the diffusion of cellular proteins through the multilayer membrane upon exposure to hypo-osmotic treatment was measured by gel electrophoresis (SDS-PAGE) (Figure 7B). The latter was performed by centrifuging the coated cells after each deposition cycle followed by analysis of the supernatant by gel electrophoresis. In general, the optimal amount of layers is considered as the number of layers that provide a stable capsular structure upon cell lysis, accompanied by minimal release of the cell lysate through the multilayer membrane.

From the fact that all cells became stained by PI, shown in Figure 7A, one can conclude that the cells are efficiently killed and lose their plasma membrane integrity upon hypo-osmotic treatment, independent of the number of deposited layers. However, only if the multilayer coating was composed of at least 3 layers (i.e., $(PVP/TA)_{1.5}$), the cells retained their spherical morphology after hypo-osmotic treatment. SDS-PAGE (Figure 7B, middle panel) performed on the supernatant of centrifuged hypo-osmotic treated cells revealed that a two bilayer coating (i.e., $(PVP/TA)_2$) allows maximum retention of cellular proteins within the capsules without further improvement when additional layers were deposited. Next, we performed SDS-PAGE on the pellet of centrifuged LbL-coated cells that were exposed to hypo-osmotic treatment in order to determine to which extend proteins are encapsulated in the bio-hybrid cell-templated capsules. In this regard, we verified that $(PVP/TA)_2$ cell-templated capsules disintegrate upon exposure to the combination of SDS, electric field and the convective flow (data not shown). Figure 7B (right panel) shows a high amount of cellular proteins in the pellet from the deposition of 1 PVP/TA bilayer onwards. Overall, one can conclude that 2 bilayers of PVP/TA offer the best solution when aiming for optimal retention, after cell lysis, of the cellular protein content into stable bio-hybrid cell-templated capsules. Figure 7D depicts electron microscopy (TEM and SEM) of these capsules, showing the presence of a continuous $(PVP/TA)_2$ membrane surrounding remnants of the cellular cytoplasm and the cell nucleus that appeared to have retained at least in parts its morphology. SEM was performed under high vacuum and further underlines the physical stability of these capsules.

2.5. Proof of Concept: Modulating the Immunogenicity via Heat Shock

Although demonstrated for inducing cell death by hypo-osmotic shock, our approach for encapsulating cell lysate can be broadly applied and also offers the opportunity to induce cell death via a number of different ways which can be attractive to modulate the immune-stimulatory properties of the cell lysate. Indeed, compelling evidence has emerged that the initiation of tumour-specific immune responses depends on how tumour cells are killed prior to uptake by antigen presenting cells.[49–51] In particular a process called immunogenic cell death has been reported to strongly boost anti-tumour immunity.[52,53] Immunogenic cell death is evoked by strong cellular stress responses and causing the dying cells to emit so-called Damage-Associated Molecular Patterns (DAMPS). As a proof of concept, we aimed at exploring whether our cell encapsulation strategy also allows to modulate cell death and to induce DAMPS. To address this, we exposed the cells prior to coating to a heat shock by incubating them during 1 h at 42 °C. Exposing cells to such heat treatment should lead to the induction of so-called heat shock proteins (HSP) that can be sensed by the immune system as a danger signal. Subsequently, the cells were cultured for an additional 24 h and then coated with a $(PVP/TA)_2$ membrane. To determine the presence of HSPs within the capsules, SDS-PAGE was performed on the capsule suspension followed by western blot analysis. As depicted in **Figure 8**, HSP90 is detected both in control cells and heat shock treated cells suggesting HSP 90 is basally present in B16.F10 cells and expression is not increased upon exposure to heat shock. In contrary HSP70 was found only in the case of pre-treated cells indicating that pre-treatment of the cells with heat shock allows us to up-regulate certain heat shock proteins and to encapsulate the induced DAMPs within the capsules.

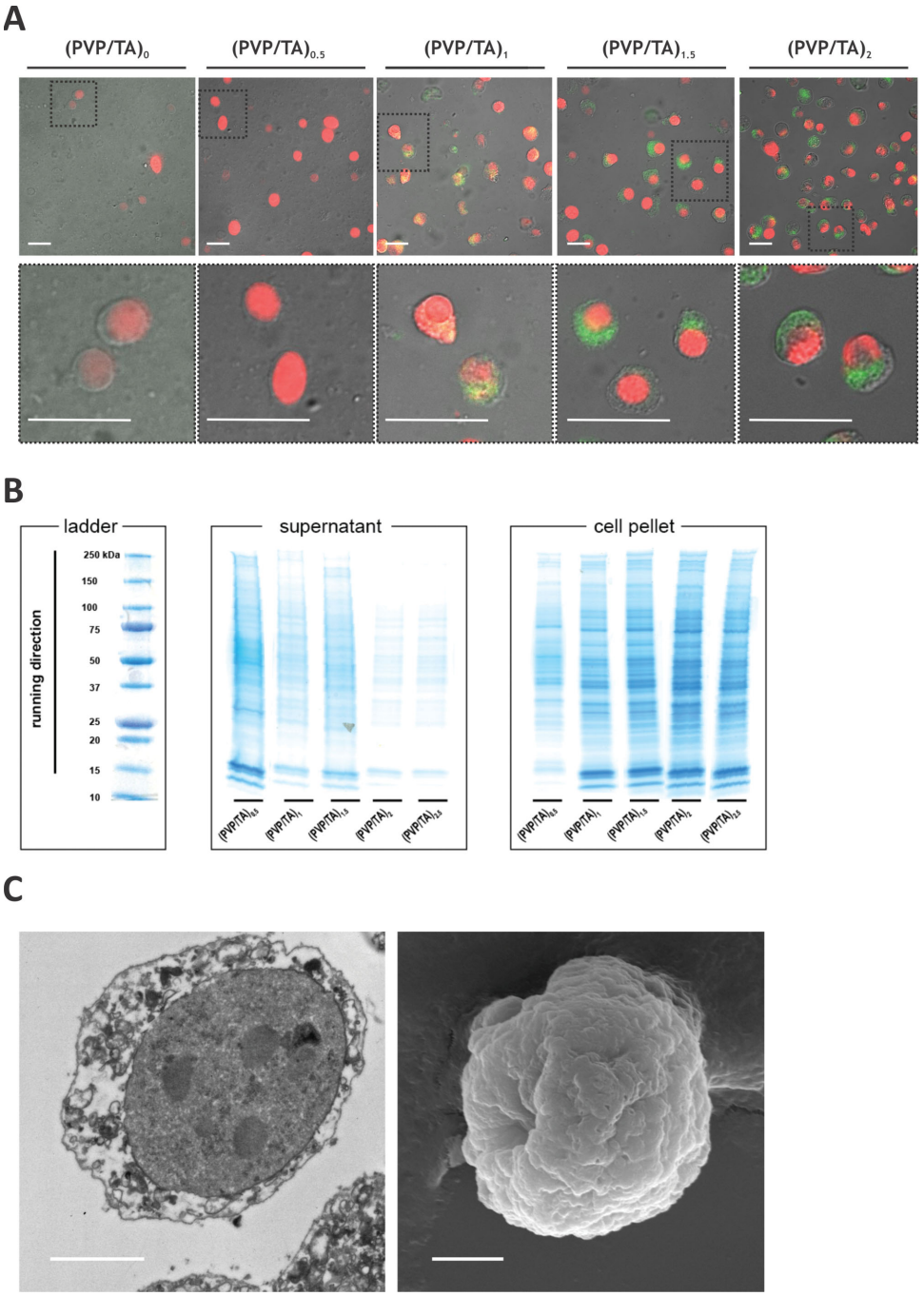

Figure 7. A) Fluorescence microscopy images of B16.F10 cells stained with C-AM/PI upon hypo-osmotic treated after Layer-by-Layer deposition of PVP/TA. The images, shown at different magnification, are an overlay of the DIC, green and red fluorescence channels. The dashed rectangles show a zoomed area. Scale bar is 20 μm. B) SDS-PAGE recorded from the supernatant and the cell pellet after hypo-osmotic treatment of the PVP/TA Layer-by-Layer coated B16.F10 cells. C) Transmission (left panel) and scanning (right panel) electron microscopy images of biohybrid cell-templated capsules obtained by hypo-osmotic treatment of $(PVP/TA)_2$ coated B16.F10 cells. Scale bar is 3 μm.

3. Conclusion

To summarize, we have demonstrated in this paper that live cancer cells can be encapsulated within a synthetic membrane composed of PVP and TA via hydrogen bonding. Fine-tuning of the assembly conditions allowed us to obtain cell-templated bio-hybrid capsules containing a high amount of encapsulated proteins. We also demonstrated, in a proof of concept study, that heat shock prior to cellular encapsulation can be employed to potentially modulate the immunogenic properties of the capsules. In our ongoing research, we are currently aiming for modification of the cell-templated capsules via exposure to salt[54] or high temperature[55] in order to induce shrinkage of the capsules and to allow more efficient uptake by immune cells. Additionally, we

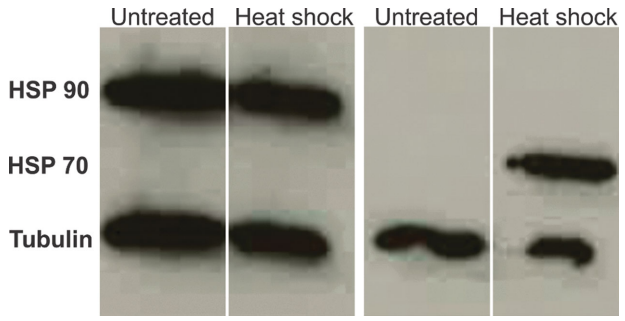

Figure 8. Western blot result of LbL coated B16.F10 cells either untreated or treated with 1 h heat shock at 42°C prior to coating. Presence of HSP within the capsules is determined by using antibodies against HSP 70 and HSP 90. Tubulin staining is included as a loading control.

plan to engineer the capsule surface with immune-stimulating cues and investigate the potential of these capsules and other cell lysate formulation strategies as delivery system for tumour-associated antigens in view of anti-cancer immune-therapy.

4. Experimental Section

4.1. Materials

Dulbecco's Modified Eagle Medium (DMEM), fetal bovine serum (EU qualified), penicillin/streptomycin (5000 U/mL), sodium pyruvate (100 mM), L-glutamine (200 mM), cell dissociation buffer (PBS based), PBS buffer (pH 7.2), Calcein-AM (CAM) and Propidium Iodide (PI) were purchased from Invitrogen. 3-(4,5-dimethylthiazol-2-yl)-2,5-diphenyltetrazolium bromide (MTT) reagent, sodium dodecyl sulfate (SDS), bovine serum albumin (BSA), Poly-L-arginine hydrochloride (Mw > 70 kDa), dextran sulfate (10 kDa) and DMSO were obtained from Sigma Aldrich. Poly(vinylpyrrolidone) (PVP) K16–18 and hydrochloric acid (HCl) 37% v/v was obtained from Fischer Scientific. Tannic acid (TA) was purchased from Fluka. 2-Mercaptoethanol, laemli sample buffer (4x), Coomassie blue stain (G-250) were purchased from Bio-rad. For western blot staining the monoclonal antibodies HSP 70 and HSP 90 α/β were respectively obtained from Enzo Life Sciences and Santa Cruz Biotechnology.

4.2. Cell Lines

B16.F10 cells (ATCC CRL-6475) were cultured in Dulbecco's Modified Eagle Medium (DMEM) supplemented with 10% fetal bovine serum, 1% penicillin/streptomycin, 1 mM sodium pyruvate and 2 mM L-glutamine and incubated at 37 °C with 5% CO_2 saturation. Isolation of the cells for experiments was performed by incubation of the cells in a PBS-based dissociation buffer for 10 minutes.

4.3. Fabrication of Bio-Hybrid Cell-Templated Capsules

B16.F10 cells were harvested and diluted to a concentration of 20×10^6 cells/mL. Cells were coated at 0 °C in a isotonic phosphate buffered saline (PBS) buffer. The cell suspension was incubated during 10 min with either one of the coating components (dextran sulfate, poly-L-arginine, tannic acid or poly(vinylpyrrolidone)) dissolved in PBS at a 1 mg/mL. The cells were subsequently centrifuged at 200 G for 5 minutes and washed two times with PBS. Subsequently, the complimentary interacting component was added and again incubated for 10 min followed by centrifugation and washing. This was repeated until the desired amount of layers was assembled. After coating, the live cells were incubated for 30 min in deionized water at room temperature in order to kill the cells.

4.4. MTT Assay

Cell viability was assessed by the 3-(4,5-dimethylthiazol-2-yl)-2,5-diphenyltetrazolium bromide (MTT) assay. Coated B16.F10 cells were seeded in 96 well plates at a density of 50000 cells/mL in complete DMEM medium (total volume 100 µL) in six-fold. Subsequently the cells were cultured for 24 h followed by addition of 40 µL of the MTT reagent (1 mg/mL). After an incubation period of 2–3 h the formed formazan crystals were dissolved in 100 µL of a 10% m/v SDS/0.01 M HCl solution overnight protected from light. The absorbance was measured by a microplate reader at 570 nm. As a negative and positive control PBS buffer and DMSO respectively were added to the wells.

4.5. Online Flow Cytometry

Online flow cytometry was performed on a BD Accuri C6 flow cytometer using the Live/dead fixable far red dead cell stain kit purchased from Invitrogen. For assessing the cell membrane integrity, cells were suspended at a density of 1×10^6 cells/mL followed by the addition of 1 µL live/dead reagent. Subsequently, the cells were placed under continuous gentle agitation on ice and the sip of the flow cytometer was immersed into the cell suspension. Next, flow cytometry was started by measuring the cells for 2 min followed by addition of the respective test components. Data were collected over 12 min on ice and processed via FlowJo.

4.6. Live/Dead Assay (offline)

Cells were suspended in a concentration of 1×10^6 cells per mL in PBS and incubated with 1 µL of live/dead reagent (purchased from Invitrogen) for 30 minutes on ice. The particles were collected by centrifugation and residual reagent was removed by washing once with 1% BSA in PBS. The percentage live versus dead cells was determined by flow cytometry.

4.7. Fluorescence Microscopy Analysis of Cell Viability

A double staining with calcein-AM (C-AM; live cell staining) and propidium iodide (PI; dead cell staining) was performed. Cells, at a density of 1×10^6 cells/mL, were incubated for 30 minutes with a mixture of C-AM and PI at a concentration of respectively 3 µM and 0.25 nM. After removal of the excess reagent, the cells were visualized by fluorescence microscopy using a Leica DM2500P equipped with a 40X (NA 0.75) objective, DIC filters and a DFC360FX camera.

4.8. Electron Microscopy

Transmission electron microscopy (TEM) was performed on a JEOL 1010 instrument. Prior to imaging, samples were subjected to series of fixation (0.1 M Na cacodylate buffer (pH 7.2) containing 4% paraformaldehyde and 2,5% glutaraldehyde) and dehydration steps, embedded in epoxy resin and cut into ultrathin section using an ultramicrotome.

Scanning electron microscopy (SEM) was performed on a Quanta 200 FEG FEI instrument. Samples were deposited onto a silicon wafer and dried under a gentle nitrogen stream at ambient temperature. Prior to imaging, the samples were sputtered with a palladium/gold coating.

4.9. Gel Electrophoresis (SDS-PAGE)

To visualize potential protein release during the LbL coating and after lysis or to evaluate the presence of proteins within the final bio-hybrid cell-templated capsules, gel electrophoresis was performed respectively on the supernatant or on the cell suspension. The samples were diluted with a 1:9 β-mercaptoethanol:laemli sample buffer solution (4×), incubated for 5 minutes at 95°C and loaded on 4–20% precast gels. After the run (150 kV), visualization of the protein bands was obtained by incubation of the gels into Coomassie blue stain.

4.10. Western Blot

To visualize expression of heat shock protein 70 (HSP70) and heat shock protein 90 (HSP 90) the samples were separated by gel electrophoresis as described above. After the run, the gels were transferred to nitrocellulose membranes and quenching was performed by incubation for 30 minutes in a blocking solution containing 5% non-fat milk and 0.5% Tween 20 in PBS. The membranes were stained with primary antibody anti-HSP90 α or anti-HSP70 and anti-α-tubulin antibody as a loading control for at least 1 hour. After rinsing the membranes three times with the blocking solution the membrane was incubated with horseradish peroxidase-conjugated anti-mouse secondary antibody for 1 hour. The membranes were subsequently rinsed three times with the blocking solution followed by rinsing three times with a 0.5% tween-20 solution in PBS. The proteins were visualized by the enhanced chemiluminescence (ECL) procedure.

Acknowledgements

This work was financially supported by the Agency for Innovation by Science and Technology in Flanders (IWT) and the FWO Flanders.

Received: July 11, 2014
Revised: August 5, 2014
Published online: September 11, 2014

[1] K. Palucka, J. Banchereau, *Nat. Rev. Cancer* **2012**, *12*, 265.
[2] S. T. Reddy, M. A. Swartz, J. A. Hubbell, *Trends Immunol.* **2006**, *27*, 573.
[3] H. A. A. Aly, *J. Immunol. Methods* **2012**, *382*, 1.
[4] I. Mellman, G. Coukos, G. Dranoff, *Nature* **2011**, *480*, 480.
[5] J. Banchereau, R. M. Steinman, *Nature* **1998**, *392*, 245.
[6] R. M. Steinman, J. Banchereau, *Nature* **2007**, *449*, 419.
[7] J. E. Boudreau, A. Bonehill, K. Thielemans, Y. Wan, *Mol. Ther.* **2011**, *19*, 841.
[8] S. Raychaudhuri, K. L. Rock, *Nat. Biotechnol.* **1998**, *16*, 1025.
[9] P. E. Jensen, *Nat. Immunol.* **2007**, *8*, 1041.
[10] S. De Koker, R. Hogenboom, B. G. De Geest, *Chem. Soc. Rev.* **2011**, *41*, 2867.
[11] M. D. Joshi, W. J. Unger, G. Storm, Y. van Kooyk, E. Mastrobattista, *J. Controlled Release* **2012**, *161*, 25.
[12] Z. H. Shen, G. Reznikoff, G. Dranoff, K. L. Rock, *J. Immunol.* **1997**, *158*, 2723.
[13] S. P. Kasturi, I. Skountzou, R. A. Albrecht, D. Koutsonanos, T. Hua, H. E. Nakaya, R. Ravindran, S. Stewart, M. Alam, M. Kwissa, F. Villinger, N. Murthy, J. Steel, J. Jacob, R. J. Hogan, A. Garcia-Sastre, R. Compans, B. Pulendran, *Nature* **2011**, *470*, 543.
[14] J. J. Moon, B. Huang, D. J. Irvine, *Adv. Mater.* **2012**, *24*, 3724.
[15] J. A. Hubbell, S. N. Thomas, M. A. Swartz, *Nature* **2009**, *462*, 449.
[16] S. Y. Liu, W. Wei, H. Yue, D. Z. Ni, Z. G. Yue, S. Wang, Q. Fu, Y. Q. Wang, G. H. Ma, Z. G. Su, *Biomaterials* **2013**, *34*, 8291.
[17] S. A. Tawde, L. Chablani, A. Akalkotkar, C. D'Souza, M. Chiriva-Internati, P. Selvaraj, M. J. D'Souza, *Vaccine* **2012**, *30*, 5675.
[18] S. Mansouri, Y. Merhi, F. M. Winnik, M. Tabrizian, *Biomacromolecules* **2011**, *12*, 585.
[19] N. G. Veerabadran, P. L. Goli, S. S. Stewart-Clark, Y. M. Lvov, D. K. Mills, *Macromol. Biosci.* **2007**, *7*, 877.
[20] Q. H. Zhao, H. S. Li, B. Y. Li, *J. Mater. Res.* **2011**, *26*, 347.
[21] A. Diaspro, D. Silvano, S. Krol, O. Cavalleri, A. Gliozzi, *Langmuir* **2002**, *18*, 5047.
[22] L. E. Kandalaft, D. J. Powell, C. L. Chiang, J. Tanyi, S. Kim, M. Bosch, K. Montone, R. Mick, B. L. Levine, D. A. Torigian, C. H. June, G. Coukos, *Oncoimmunology* **2013**, *2*, e22664.
[23] U. E. Burkhardt, U. Hainz, K. Stevenson, N. R. Goldstein, M. Pasek, M. Naito, D. Wu, V. T. Ho, A. Alonso, N. N. Hammond, J. Wong, Q. L. Sievers, A. Brusic, S. M. McDonough, W. Y. Zeng, A. Perrin, J. R. Brown, C. M. Canning, J. Koreth, C. Cutler, P. Armand, D. Neuberg, J. S. Lee, J. H. Antin, R. C. Mulligan, T. Sasada, J. Ritz, R. J. Soiffer, G. Dranoff, E. P. Alyea, C. J. Wu, *J. Clin. Invest.* **2013**, *123*, 3756.
[24] P. J. Tacken, I. J. de Vries, R. Torensma, C. G. Figdor, *Nat. Rev. Immunol.* **2007**, *7*, 790.
[25] D. Avigan, *Clin. Cancer Res.* **2004**, *10*, 6347S.
[26] A. E. Chang, B. G. Redman, J. R. Whitfield, B. J. Nickoloff, T. M. Braun, P. P. Lee, J. D. Geiger, J. J. Mulé, *Clin. Cancer Res.* **2002**, *8*, 1021.
[27] T. Kamigaki, T. Kaneko, K. Naitoh, M. Takahara, T. Kondo, H. Ibe, E. Matsuda, R. Maekawa, S. Goto, *Anticancer Res.* **2013**, *33*, 2971.
[28] R. Yamanaka, J. Honma, N. Tsuchiya, N. Yajima, T. Kobayashi, R. Tanaka, *J. Neuro-oncol.* **2005**, *72*, 107.
[29] G. Decher, *Science* **1997**, *277*, 1232.
[30] J. Flemke, M. Maywald, V. Sieber, *Biomacromolecules* **2013**, *14*, 207.
[31] J. L. Carter, I. Drachuk, S. Harbaugh, N. Kelley-Loughnane, M. Stone, V. V. Tsukruk, *Macromol. Biosci.* **2011**, *11*, 1244.
[32] V. Kozlovskaya, S. Harbaugh, I. Drachuk, O. Shchepelina, N. Kelley-Loughnane, M. Stone, V. V. Tsukruk, *Soft Matter* **2011**, *7*, 2364.
[33] R. F. Fakhrullin, Y. M. Lvov, *ACS Nano* **2012**, *6*, 4557.
[34] B. G. De Geest, R. E. Vandenbroucke, A. M. Guenther, G. B. Sukhorukov, W. E. Hennink, N. N. Sanders, J. Demeester, S. C. De Smedt, *Adv. Mater.* **2006**, *18*, 1005.
[35] S. De Koker, B. G. De Geest, C. Cuvelier, L. Ferdinande, W. Deckers, W. E. Hennink, S. De Smedt, N. Mertens, *Adv. Funct. Mater.* **2007**, *17*, 3754.
[36] B. G. De Geest, M. A. Willart, H. Hammad, B. N. Lambrecht, M. De Filette, X. Saelens, J. P. Remon, J. Grooten, S. De Koker, *ACS Nano* **2012**, *6*, 2136.
[37] B. G. De Geest, M. A. Willart, B. N. Lambrecht, C. Vervaet, J. P. Remon, J. Grooten, S. De Koker, *Angew. Chem.* **2012**, *51*, 3862.
[38] S. De Koker, T. Naessens, B. G. De Geest, P. Bogaert, J. Demeester, S. De Smedt, J. Grooten, *J. Immunol.* **2010**, *184*, 203.
[39] L. J. De Cock, J. Lenoir, S. De Koker, V. Vermeersch, A. G. Skirtach, P. Dubruel, E. Adriaens, C. Vervaet, J. P. Remon, B. G. De Geest, *Biomaterials* **2011**, *32*, 1967.
[40] V. Kozlovskaya, E. Kharlampieva, I. Drachuk, D. Cheng, V. V. Tsukruk, *Soft Matter* **2010**, *6*, 3596.
[41] Y. Guan, S. Yang, Y. Zhang, J. Xu, C. C. Han, N. A Kotov, *J. Phys. Chem. B* **2006**, *110*, 13484.
[42] L. Zhou, M. Chen, L. Tian, Y. Guan, Y. Zhang, *ACS Appl. Mater. Interfaces* **2013**, *5*, 3541.
[43] M. Dierendonck, K. Fierens, R. De Rycke, L. Lybaert, S. Maji, Z. Zhang, Q. Zhang, R. Hoogenboom, B. N. Lambrecht, J. Grooten,

J. P. Remon, S. De Koker, B. G. De Geest, *Adv. Funct. Mater.* **2014**, *24*,4634.
[44] H. Ejima, J. J. Richardson, K. Liang, J. P. Best, M. P van Koeverden, G. K. Such, J. Cui, F. Caruso, *Science* **2013**, *341*, 154.
[45] T. S. Sileika, D. G. Barrett, R. Zhang, K. H. A. Lau, P. B. Messersmith, *Angew. Chem.* **2013**, *52*, 10766.
[46] H. Lee, S. M. Dellatore, W. M. Miller, P. B. Messersmith, *Science* **2007**, *318*, 426.
[47] J. L. Carter, I. Drachuk, S. Harbaugh, N. Kelley-Loughnane, M. Stone, V. V. Tsukruk, *Macromol. Biosci.* **2011**, *11*, 1244.
[48] J. T. Wilson, C. Wanxing, V. Kozlovskaya, E. Kharlampieva, D. Pan, Z. Qu, V. R. Krishnamurthy, J. Mets, V. Kumar, J. Wen, Y. Song, V. V. Tsukruk, E. L. Chaikof, *J. Am. Chem. Soc.* **2011**, *133*, 705.
[49] R. Aguilera, C. Saffie, A. Tittarelli, F. E. Gonzalez, M. Ramirez, D. Reyes, C. Pereda, D. Hevia, T. Garcia, L. Salazar, A. Ferreira, M. Hermoso, A. Mendoza-Naranjo, C. Ferrada, P. Garrido, M. N. Lopez, F. Salazar-Onfray, *Clin. Cancer Res.* **2011**, *17*, 2474.
[50] S. Knudsen, A. Schardt, T. Buhl, L. Boeckmann, M. P. Schön, C. Neumann, H. A. Haenssle, *Exp. Dermatol.* **2009**, *19*, 108.
[51] T. Imai, Y. Kato, C. Kajiwara, S. Mizukami, I. Ichiyanagi, M. Hikida, J. Wang, H. udono, *Proc. Natl. Acad. Sci. USA* **2011**, *39*, 16363.
[52] G. Kroemer, L. Galluzzi, O. Kepp, L. Zitvogel, *Annu. Rev. Immunol.* **2013**, *31*, 51.
[53] D. V. Krysko, A. D. Garg, A. Kaczmarek, O. Krysko, P. Agostinis, P. Vandenabeele, *Nat. Rev. Cancer* **2012**, *12*, 860.
[54] K. Kohler, P. M. Biesheuvel, R. Weinkamer, H. Mohwald, G. B. Sukhorukov, *Phys. Rev. Lett.* **2006**, *97*, 188301.
[55] K. Kohler, D. G. Shchukin, G. B. Sukhorukov, H. Mohwald, *Macromolecules* **2004**, *37*, 9546.